Synthesis, structure, magnetic properties and DNA cleavage of binuclear Cu(II) Schiff-base complexes†

Yingying Kou, Jinlei Tian,* Dongdong Li, Wen Gu, Xin Liu, Shiping Yan,* Daizheng Liao and Peng Cheng

Received 28th October 2008, Accepted 16th December 2008
First published as an Advance Article on the web 9th February 2009
DOI: 10.1039/b819052f

Five binuclear Schiff base copper(II) complexes $[Cu_2(L)(OAc)]\cdot 3DMF$ (**1**), $[Cu_2(L)(OAc)]_2\cdot 3DMF$ (**2**), $[Cu_2(L)(BNPP)]\cdot 3CH_3CN$ (**3**), $[Cu_2(L)(Fa)]\cdot 2DMF$ (**4**) and $[Cu_2(L)(Pa)]\cdot DMF$ (**5**) (H_3L = *N*,*N*′-bis(3,5-*tert*-butylsalicylidene-2-hydroxy)-1,3-propanediamine, OAc = acetic acid, BNPP = bis(4-nitrophenyl)phosphate, Fa = 2-tetrahydrofuroic acid, Pa = benzoic acid) have been synthesized and characterized by X-ray single-crystal structure analysis. Variable-temperature magnetic susceptibility studies (2–300 K) indicate the existence of ferromagnetic coupling between the copper(II) ions in complexes **1** and **4**, and antiferromagnetic coupling in complexes **3** and **5**. The interaction of these complexes with CT-DNA has been studied by using absorption and emission spectral methods. The apparent binding constant (K_{app}) values for complexes **1**, **3**, **4** and **5** are 4.67×10^5, 9.48×10^5, 4.30×10^5 and 3.90×10^5 M^{-1}, respectively, which show that the complexes bind to DNA by moderate intercalative binding modes. Furthermore, all these complexes can cleave plasmid DNA to nicked DNA in a sequential manner as the concentrations or reaction times are increased in the absence of reducing agent. Their cleavage activities are promoted in the presence of hydrogen peroxide. The cleavage mechanisms between the complexes and plasmid DNA are likely to involve singlet oxygen $^1O_2$ and $^{\bullet}OH$ as reactive oxygen species.

Introduction

Nuclease molecules which cleave the DNA duplex have been a significant topic of interest for biochemists. Natural nucleases cleave the phosphate diester backbone of DNA by hydrolysis,[1] while chemical nucleases cleave DNA by oxidatively degrading the deoxyribose moiety[2] or by hydrolysis of the phosphate ester.[3] The study of artificial nucleases has received attention for their diverse applications not only as chemical therapeutic agents but also in genomic research over several decades.[4–8] Chemical nucleases present some advantages over conventional enzymatic nucleases in that they are smaller in size and thus can reach more sterically hindered regions of a macromolecule. Many of these utilize the redox properties of the metal and dioxygen to produce reactive oxygen species that oxidize DNA, yielding direct strand scission or base modification.[9] In this regard, transition-metal complexes, especially copper complexes play an important role due to their structural diversity. Copper complexes are capable of cleaving DNA by both the hydrolytic and oxidative cleavage modes, the best studied of these being $[Cu(phen)_2]^{2+}$ which induces direct strand damage in the presence of H_2O_2.[10] Three equivalents of the Cu(II) species are required for this process to produce a non-diffusible intermediate equivalent to a hydroxyl radical. This fact has focused large attention on copper compounds due to their potential for efficient intramolecular activation of bound O_2 and for binding in a selective manner to particular nucleic acid conformations.[11]

Besides the interest of copper compounds related to nucleases, polynuclear copper compounds have attracted much attention due to their coupling interactions of multicopper centers in biological systems. As far as we know, most of the bi-bridge binuclear copper(II) systems, for example μ-hydroxo/alkoxo-μ-X (X = carboxylato) systems, are antiferromagnetically coupled, whereas ferromagnetic interaction has been observed in only a few μ-hydroxo/alkoxo-μ-carboxylato compounds.[12–15] In general, most of the μ-alkoxo-X bridged Cu(II) complexes show ferromagnetic exchange for a Cu–O–Cu angle lower than 116.5° and are antiferromagnetic above this value.[16]

Recently we have begun to explore the nuclease activity of binuclear Cu(II) complexes.[17,18] Moreover, because of our interest in the binuclear/polynuclear copper(II) complexes, we have reported the crystal structures and spectroscopic and magnetic properties of binuclear copper(II) complexes. Here, we present five new binuclear copper(II) complexes of Schiff-base ligands (H_3L) with alkoxo and carboxylato or phosphato bridges. The single-crystal structures and magnetic properties and DNA cleavage activities of these complexes, which efficiently cleave DNA in the presence of H_2O_2, have been studied.

Results and discussion

X-Ray crystal structure characterization

The crystal structures of complexes **1–5** were determined and are shown in Fig. 1–5, respectively. Selected bond distances and bond angles are listed in Table 2.

Department of Chemistry, Nankai University, Weijin Road 94, Tianjin, 300071, P. R. China. E-mail: yansp@nankai.edu.cn.

† Electronic supplementary information (ESI) available: Additional characterization data (Table S1, Fig. S1–S4). CCDC reference numbers 673944 (**1**), 702845 (**2**), 680010 (**3**), 697012 (**4**) and 697013 (**5**). For ESI and crystallographic data in CIF or other electronic format see DOI: 10.1039/b819052f

Table 1 Crystal data and structure refinement for all compounds

Complex	**1**	**2**	**3**	**4**	**5**
Empirical formula	$C_{44}H_{73}Cu_2N_5O_8$	$C_{79}H_{121}Cu_4N_7O_{13}$	$C_{51}H_{64}Cu_2N_7O_{11}P$	$C_{44}H_{68}Cu_2N_4O_8$	$C_{43}H_{58.50}Cu_2N_3O_6$
M_r	927.15	1630.99	1109.14	908.10	840.51
T/K	113(2)	113(2)	293(2)	113(2)	113(2)
λ/Å	0.71073	0.71073	0.71073	0.71073	0.71073
Crystal system	Triclinic	Triclinic	Triclinic	Monoclinic	Triclinic
Space group	$P\bar{1}$	$P\bar{1}$	$P\bar{1}$	$P2_1/n$	$P\bar{1}$
a/Å	9.972(2)	13.670(3)	10.718(2)	19.524(4)	16.615(3)
b/Å	14.743(4)	16.814(3)	15.912(3)	9.7034(19)	16.617(3)
c/Å	17.732(5)	19.012(4)	17.567(4)	24.564(5)	17.076(3)
α/°	108.293(3)	99.93(3)	102.90(3)	90	102.19(3)
β/°	91.948(2)	97.97(3)	107.26(3)	97.33(3)	99.22(3)
γ/°	90.183(3)	98.08(3)	92.94(3)	90	106.83(3)
V/Å^3	2473.5(10)	4201.8(15)	2766.5(10)	4615.5(16)	4285.5(15)
Z	2	2	2	4	4
D_c/g cm^{-3}	1.245	1.289	1.331	1.307	1.303
μ/mm^{-1}	0.911	1.060	0.860	0.975	1.040
$F(000)$	988	1728	1160	1928	1774
Crystal size/mm	0.20 × 0.20 × 0.20	0.20 × 0.18 × 0.12	0.12 × 0.10 × 0.08	0.12 × 0.10 × 0.08	0.20 × 0.16 × 0.12
θ Range for data collection/°	2.04–25.01	2.03–25.02	1.58–25.02	1.42–27.57	1.26–25.02
Reflections collected/unique	21731/8694	24583/14715	16379/9614	32086/10621	24573/14922
R_{int}	0.0338	0.0273	0.0968	0.0461	0.0807
Max./min. transmission	0.8388/0.8388	0.8834/0.8160	0.9344/0.9039	0.9261/0.8920	0.8853/0.8189
Data/restraints/parameters	8694/0/552	14715/162/1004	9614/0/664	10621/357/634	14922/72/1028
Goodness of fit on F^2	1.082	1.024	1.006	1.039	1.082
Final R indices [$I > 2\sigma(I)$]	$R_1 = 0.0485$, $wR_2 = 0.1273$	$R_1 = 0.0383$, $wR_2 = 0.0979$	$R_1 = 0.0843$, $wR_2 = 0.1887$	$R_1 = 0.0472$, $wR_2 = 0.1239$	$R_1 = 0.0809$, $wR_2 = 0.2170$
R indices (all data)	$R_1 = 0.0549$, $wR_2 = 0.1329$	$R_1 = 0.0481$, $wR_2 = 0.1040$	$R_1 = 0.1092$, $wR_2 = 0.2115$	$R_1 = 0.0606$, $wR_2 = 0.1331$	$R_1 = 0.1077$, $wR_2 = 0.2307$
$\Delta\rho$(max./min.)/e Å^{-3}	1.364/–0.746	0.816/–0.720	1.483/–1.938	0.934/–0.728	1.171/–0.825

Table 2 Selected bond lengths (Å) and angles (°) for all compounds

Complex	**1**	**2**	**3**	**4**	**5**
Cu(1)–N(1)	2.000(2)	1.927(2)	1.915(4)	1.929(2)	1.931(5)
Cu(1)–O(1)	1.916(2)	1.9020(18)	1.920(4)	1.8967(17)	1.881(4)
Cu(1)–O(2)	1.953(2)	1.9570(18)	1.973(4)	1.9408(17)	1.904(4)
Cu(1)–O(4)	1.983(2)	1.9603(19)	1.954(4)		1.937(5)
Cu(1)–O(5)				1.9585(18)	
Cu(2)–N(2)	1.983(2)	1.922(2)	1.934(4)	1.915(2)	1.923(5)
Cu(2)–O(2)	1.927(2)	1.9430(19)	1.954(4)	1.9699(17)	1.921(5)
Cu(2)–O(3)	1.887(2)	1.8967(19)	1.901(4)	1.9072(18)	1.895(5)
Cu(2)–O(5)	1.949(2)	1.938(2)	1.956(3)		1.958(4)
Cu(2)–O(4)				1.9536(18)	
O(1)–Cu(1)–O(2)	174.22(9)	175.52(8)	177.62(14)	175.00(7)	175.6(2)
O(1)–Cu(1)–O(4)	90.40(8)	89.19(8)	88.56(15)		88.0(2)
O(1)–Cu(1)–N(1)	93.10(9)	93.13(9)	92.57(16)	91.42(8)	92.5(2)
O(1)–Cu(1)–O(5)				88.60(7)	
O(2)–Cu(1)–O(4)	90.16(8)	94.04(8)	93.23(14)		94.8(2)
O(2)–Cu(1)–N(1)	84.90(9)	84.67(9)	85.56(16)	85.22(8)	85.1(2)
O(2)–Cu(1)–O(5)				93.95(7)	
O(5)–Cu(1)–N(1)				168.54(8)	
O(4)–Cu(1)–N(1)	164.61(9)	163.28(9)	177.03(16)		173.6(2)
O(2)–Cu(2)–O(4)				92.83(8)	
O(2)–Cu(2)–O(5)	90.72(9)	178.78(9)	95.69(15)		95.25(19)
O(2)–Cu(2)–N(2)	86.60(9)	85.70(9)	85.55(16)	85.06(8)	83.9(2)
O(3)–Cu(2)–O(2)	174.77(10)	168.34(8)	173.65(14)	170.50(7)	174.4(2)
O(3)–Cu(2)–O(4)				89.54(8)	
O(3)–Cu(2)–O(5)	89.29(9)	87.97(8)	86.88(15)		88.50(19)
O(3)–Cu(2)–N(2)	94.35(10)	92.59(9)	93.12(16)	92.40(8)	93.1(2)
O(4)–Cu(2)–N(2)				177.70(9)	
O(5)–Cu(2)–N(2)	168.96(10)	178.78(9)	168.14(17)		170.0(2)
Cu(1)–O(2)–Cu(2)	107.06(4)	105.60(9)	137.75(9)	105.48(4)	128.25(6)
Cu(3)–O(8)–Cu(4)		105.45(8)			

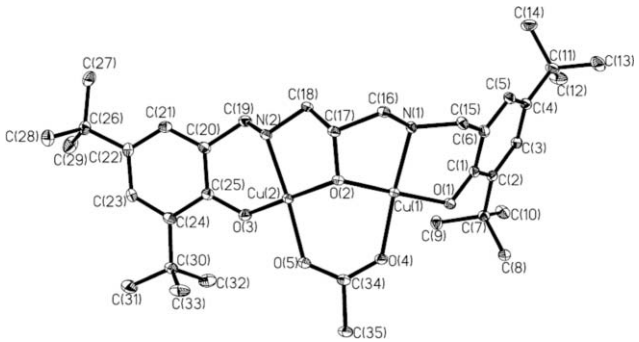

Fig. 1 ORTEP view of the molecular structure and atom-labeling scheme of **1**. Hydrogen atoms and DMF are omitted for clarity.

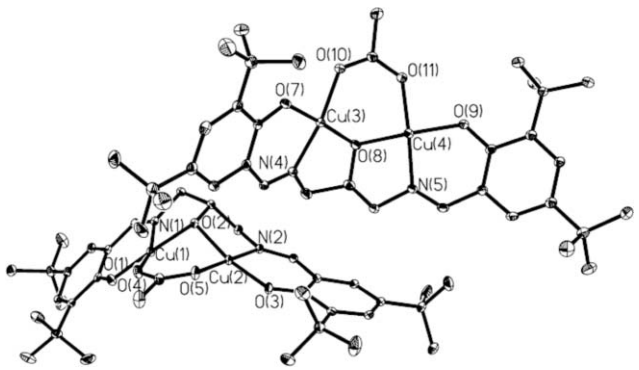

Fig. 2 ORTEP view of the molecular structure and atom-labeling scheme of **2**. Hydrogen atoms and DMF are omitted for clarity.

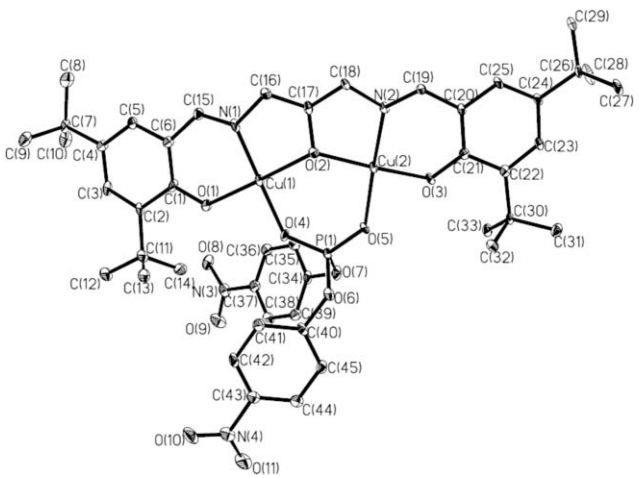

Fig. 3 ORTEP view of the molecular structure and atom-labeling scheme of **3**. Hydrogen atoms and CH_3CN are omitted for clarity.

In general, the crystal structures of the complexes **1** and **2** are found to be similar, while the complex **2** contains two independent molecules in the crystallographic asymmetric unit. The structure **1** (Fig. 1) shows that the two copper centers are doubly bridged by the alkoxo oxygen and the acetate anion. The coordination geometry around each of the copper atoms is distorted square planar, and formed by one μ-alkoxo oxygen, one-μ-acetate oxygen, one imine nitrogen and one phenoxo oxygen afforded by the ligand L^{3-}. The displacements of the copper atoms from the respective least-squares N_1O_3 coordination planes are only small:

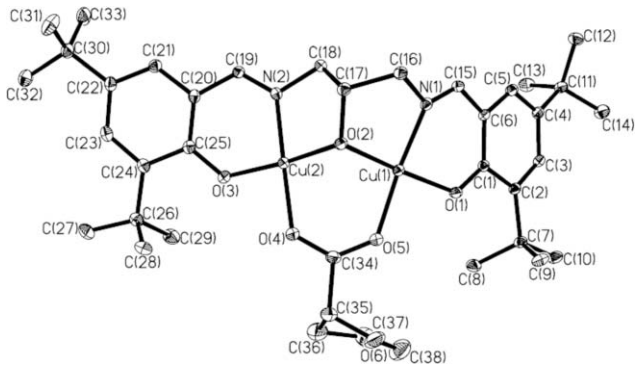

Fig. 4 ORTEP view of the molecular structure and atom-labeling scheme of **4**. Hydrogen atoms and DMF are omitted for clarity.

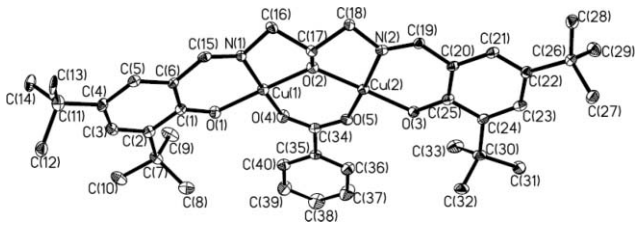

Fig. 5 ORTEP view of the molecular structure and atom-labeling scheme of **5**. Hydrogen atoms and DMF are omitted for clarity.

for **1**: 0.176 Å (Cu(1)) and 0.047 Å (Cu(2)), respectively, and for **2**: 0.111 Å (Cu(1)), 0.087 Å (Cu(2)), 0.116 Å (Cu(3)) and 0.040 Å (Cu(4)). The dihedral angle between the best coordination planes in Cu(1)Cu(2) and Cu(3)Cu(4) dinuclear units is 62.6° for **1** and 60.8° and 63.7° for **2**, respectively. The twisting is also reflected in the smaller values of Cu–O(alkoxo)–Cu bridging angles (θ) (Cu(1)–O(2)–Cu(2) = 107.06° for **1** and Cu(1)–O(2)–Cu(2) = 105.60° and Cu(3)–O(8)–Cu(4) = 105.45° for **2**), and the shorter separations (Cu(1)···Cu(2) = 3.120 Å for **1** and Cu(1)···Cu(2) = 3.107 Å, Cu(3)···Cu(4) = 3.114 Å for **2**, respectively) of the metal centers within the dinuclear units are observed related to analogues.[14,19]

The molecular structures of **3–5** are essentially similar to that of **1**. The maximum deviations of the copper atoms from the mean basal planes are 0.036 Å (Cu(1)) and 0.050 Å (Cu(2)) for **3**; 0.131 Å (Cu(1)) and 0.087 Å (Cu(2)) for **4** and 0.024 Å (Cu(1)) and 0.046 Å (Cu(2)) for **5**, respectively. The dihedral angles between the best coordination planes in Cu(1)Cu(2) dinuclear units are 10.5° for **3**, 58.3° for **4** and 25.4° for **5**, respectively. The Cu···Cu distances and Cu–O(alkoxo)–Cu angles (θ) are 3.663 Å and 137.75° for **3**, 3.112 Å and 105.48° for **4** and 3.441 Å and 128.25° for **5**, respectively.

Magnetic properties and ESR spectra

Variable-temperature (2–300 K) magnetic behavior in the form of $\chi_M T$ *vs.* T plots of **1**, **3**, **4** and **5** is shown in Fig. 6. The $\chi_M T$ values at 300 K are 0.84 $cm^3\ mol^{-1}$ K for **1** and 0.81 $cm^3\ mol^{-1}$ K for **4**, respectively, which are slightly higher than the calculated value (0.75 $cm^3\ mol^{-1}$ K, $g = 2$) of two uncoupled spins of $S = 1/2$. On lowering the temperature from 300 to 24 K for **1** and 100 K for **4**, $\chi_M T$ slowly increases and reaches a maximum value of 0.99 and 0.87 $cm^3\ mol^{-1}$ K, respectively, and then decreases

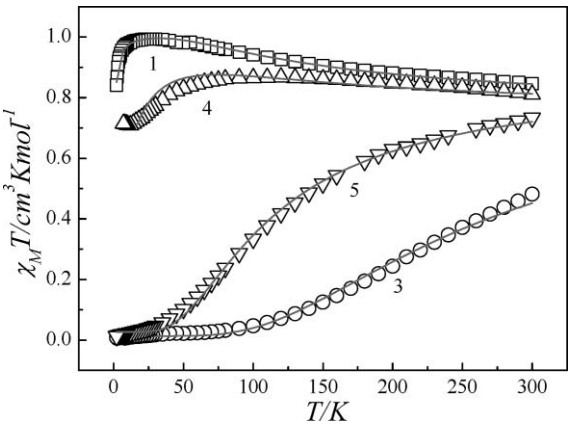

Fig. 6 $\chi_M T$ *vs.* T plots for complexes **1** (□), **3** (○), **4** (△) and **5** (▽). Solid lines represent the best theoretical fits.

rapidly on further cooling. The rapid decrease of $\chi_M T$ may be due to intermolecular antiferromagnetic interaction, which is very common in ferromagnetically coupled systems. The profiles indicate the existence of intramolecular ferromagnetic exchange interaction between the copper(II) ions in complexes **1** and **4**. In contrast, the magnetic behavior of the complexes **3** and **5**, is typical of intramolecular antiferromagnetic exchange interaction. In this case, the $\chi_M T$ values: 0.48 cm^3 mol^{-1} K for **3** and 0.73 cm^3 mol^{-1} K for **5** at 300 K are lower than that (0.75 cm^3 mol^{-1} K) of the non-correlated system of two $S = 1/2$ spins carriers. On lowering temperature, $\chi_M T$ decreases gradually to 0.0085 cm^3 mol^{-1} K for **3** and 0.0126 cm^3 mol^{-1} K for **5** at 2 K.

Taking into account the dinuclear copper model, the magnetic susceptibilities of complex can be fitted accordingly by eqn (2) derived from the Bleaney–Bowers equation $H = -2JS_1 \cdot S_2$ ($S_1 = S_2 = 1/2$).

$$\chi_M' = (1-\rho)\frac{2Ng^2\beta^2}{kT} \times \frac{1}{3 + e^{-2J/kT}} + \frac{Ng^2\beta^2}{2kT}\rho \quad (1)$$

$$\chi_M = \frac{\chi_M}{1 - 7.6853zJ'\chi_M / g^2} \quad (2)$$

Here J is the exchange coupling parameter between S_1 and S_2, ρ is the contribution of mononuclear impurity, and other symbols have their normal meanings.

There are ferromagnetic couplings between the copper(II) ions in complexes **1** and **4** and the susceptibility data can be simulated well with the equation with the following set of converging parameters: J = 56.24 cm^{-1}, g = 2.01 and zJ' = –0.19 cm^{-1} for **1**; J = 50.48 cm^{-1}, g = 2.00, ρ = 2% and zJ' = –3.50 cm^{-1} for **4**. These ferromagnetic interactions between the Cu^{2+} ions are probably due to the lower Cu–O(alkoxo)–Cu angles (θ) of 107.06° for **1** and 105.48° for **4**, respectively (<116.5°). In addition, complexes **3** and **5** show antiferromagnetic couplings as a result of the greater Cu–O(alkoxo)–Cu angles (θ) of 137.75° for **3** and 128.25° for **5** (>116.5°). The exchange parameters represent typical fits with $J = -169.23\ cm^{-1}$, $g = 2.19$ and $\rho = 1.5\%$ for **3**, and $J = -71.38\ cm^{-1}$, $g = 2.18$ and $\rho = 3\%$ for **5**.

A number of μ-alkoxo compounds have been structurally and magnetically studied to reveal the orbital complementarity effect.[14,20] We can list the magnetic properties of **1**, **3**, **4** and **5** and previously reported complexes[21,22] in a comparative fashion as shown in Table 3. The magnetic behaviors of μ-alkoxo complexes are closely related with the Cu–O–Cu bridge angles (θ). According to the linear fitting result between the Cu–O–Cu bridge angles and the $2J$ of known complexes, the magnetic exchange is ferromagnetic below 116.5° and antiferromagnetic above this value.[14] For **1**, **3**, **4** and **5**, their magnetic behaviors are all in accord with this rule.

Table 3 Variable-temperature magnetic parameters for the complexes **1**, **3**, **4** and **5** comparing previous reported

Complex	θ/°	g	J	zJ'
1	107.06(4)	2.01	56.24	–0.19
4	105.48(4)	2.00	50.48	–3.50
3	137.75(9)	2.19	–169.23	0
5	128.25(6)	2.18	–71.38	0
Cu_2(L-F)(μ-$C_7H_5N_2$)[26]	112.0(2)	2.04	26	–0.35
[Cu_2(L-H)(μ-$C_7H_5N_2$)]·CH_3OH[26]	114.3(3)	2.007	16.7	–0.82
$Cu_2(L^1)$(μ-HCO_2)[28]	132.85	2.075	–156	0
$Cu_2(L^1)$(μ-HCO_2)·DMF[28]	131.47	2.00	–152	0

Table 4 ESR parameters for complexes **1**, **3**, **4** and **5** in the solid state at room temperature

Complex	g_1 ($g_\parallel$)	g_2	g_3 ($g_\perp$)	G
1	2.205	2.070	2.053	3.87
3	2.275	2.137	2.106	2.59
4	2.236	2.112	2.096	2.46
5	2.172	2.070	2.062	2.77

The ESR spectra of complexes **1**, **3**, **4** and **5** in the solid state were measured at room temperature (Fig. S1, ESI†). No hyperfine structure is observed for any of the complexes. The spectra are quite similar and exhibit g-tensor parameters with $g_\parallel > g_\perp >$ 2.0023 (Table 4). This indicates that the copper site has a $d_{x^2-y^2}$ ground state[23] characteristic for a square-planar geometry.[24,25] Also, the observed value, which is <2.3, indicates the covalent nature between the Cu(II) ion and the ligand.[26,27]

In axial symmetry, $G = (g_\parallel - 2)/(g_\perp - 2)$ where G is the exchange interaction parameter. The calculated G values of the Cu(II) complexes are lower than 4 suggesting copper–copper exchange interactions.[24]

DNA binding properties by UV titration and competitive fluorescence displacement assay

DNA binding is the critical step for DNA cleavage in most cases. Therefore, the binding of complexes **1**, **3**, **4** and **5** to CT-DNA were studied by using UV-Vis absorption and fluorescence spectroscopy. Electronic absorption spectroscopy is one of the most useful techniques for DNA-binding studies of metal complexes. The absorption spectra of copper(II) complexes in the absence and presence of CT-DNA at different concentrations are given in Fig. S2 (ESI†). The absorption peaks with maxima of 210 nm are attributed to intraligand π–π* transitions. The intense ligand based (π–π*) absorption band is used to monitor the interaction of the complexes with calf thymus DNA. Complexes bound to DNA through intercalation, which involves a strong stacking interaction of the planar aromatic rings of the coordinated ligand with the base pairs of DNA, usually result in hypochromism and red

Table 5 Change in spectral features of the copper(II) complexes on interaction with CT-DNA in 50 mM Tris-HCl/18 mM NaCl buffer (pH = 7.2)

Complex	Change in absorptivity	λ_{max}/nm	$\Delta\lambda_{max}$/nm	$\Delta\varepsilon$ (%)
1	Hypochromism	208	4	33.85
3	Hypochromism	212	6	44.26
4	Hypochromism	218	6	35.75
5	Hypochromism	218	6	37.55

shift of ligand-band or charge-transfer bands.[28] All the present complexes exhibit significant hypochromism (33.85–44.26%) on the incremental addition of DNA with varying red shifts (Fig. S2, ESI;† Table 5). Furthermore, as the extent of hypochromism is commonly consistent with the strength of intercalative interaction, this indicates that complex **3** exhibits better DNA binding affinity compared with complexes **1**, **4** and **5**.

As a means for further clarifying the binding of complexes, fluorescence spectral measurements were carried out. The addition of complex to the DNA bound EB solutions caused obvious reduction in emission intensities, indicating that complex competitively bound to DNA with EB. The extent of reduction of the emission intensity gives a measure of the binding propensity of the complex to DNA. According to the classical Stern–Volmer equation[29] $I_0/I = 1 + K[Q]$; I_0 and I are the fluorescence intensities in the absence and presence of the quencher, respectively. K is a linear Stern–Volmer quenching constant. [Q] is the concentration of the quencher. The quenching plots (Fig. S3, ESI†) illustrate that the quenching of EB bound to DNA by complexes are in agreement with the linear Stern–Volmer equation, which also indicate the complexes bind to DNA. In the plot of I_0/I *vs.* the concentrations of complexes, K is given by the ratio of the slope to intercept. According to the equation $K_{EB}[EB] = K_{app}[complex]$, where the complex concentration is the value for a 50% reduction of the fluorescence intensity of EB ($K_{EB} = 1.0 \times 10^7$ M^{-1}, [EB] = 4.0 μM) the K_{app} values are calculated to be 4.67×10^5, 9.48×10^5, 4.30×10^5 and 3.90×10^5 M^{-1} for complexes **1**, **3**, **4** and **5**, less than the binding constant of the classical intercalators and metallointercalators (10^7 M^{-1}),[17] which suggest that the interactions of the complexes with DNA are all moderate intercalative modes. Complex **3** is the best binding agent due to its highest planarity.[30]

Electrochemical studies

Typical cyclic voltammetry (CV) behaviors of complexes in the absence and presence of CT-DNA are measured. In the presence of CT-DNA, the cyclic voltammograms of the four copper(II) complexes **1**, **3**, **4** and **5** exhibited significant shifts in the anodic and cathodic peak potentials followed by decrease in both peak currents, indicating the interaction existing between the four copper(II) complexes and CT-DNA. The E_{pa}, E_{pc}, $E_{1/2}$ values and negative shifts (ΔE) for the four copper(II) complexes **1**, **3**, **4** and **5** in the absence and presence of CT-DNA are shown in Table 6. The results indicated reversible redox processes (ΔE_p of 59 mV for a one-electron diffusion and $i_{pc} = i_{pa}$ of about 1 for a controlled reversible process). The drop of the voltammetric currents in the presence of CT-DNA can be attributed to diffusion of the metal complex bound to the large, slowly diffusing DNA molecule.[31]

Table 6 The E_{pa}, E_{pc}, $E_{1/2}$ and ΔE values for the copper(II) complexes in the absence and presence of CT-DNA

Complex	E_{pa}/mV	E_{pc}/mV	$E_{1/2}$/mV	ΔE^a/mV
1	20, –27	–62, –99	–21, –63	42
3	19, –36	–49, –100	–15, –68	53
4	5, –14	–77, –98	–36, –56	20
5	0, –31	–70, –99	–35, –65	30

[a] ΔE indicates the negative shifts for the four copper(II) complexes in the absence and presence of CT-DNA.

pBR322 DNA cleavage by the copper(II) complexes

The chemical nuclease activities of the complexes have been studied using supercoiled pBR322 plasmid DNA in a medium of 50 mM Tris-HCl/NaCl buffer (pH = 7.2) in the absence of reducing agent under similar physiological conditions. When circular plasmid DNA is conducted by electrophoresis, the fastest migration will be observed for the supercoiled form (Form I). If one strand is cleaved, the supercoils will relax to produce a slower-moving nicked circular form (Form II). If both strands are cleaved, a linear form (Form III) will be generated that migrates at a rate between that of Form I and Form II. Fig. 7 shows the results of gel electrophoretic separations of plasmid pBR322 DNA induced by an increasing concentration of complexes in the absence of reducing agent. As shown in Fig. 7, with the increase of the concentrations of the complexes, Form I plasmid DNA is gradually converted into Form II. In addition, the oxidative cleavage of DNA in the presence of hydrogen peroxide has also been studied by gel electrophoresis and shown in Fig. 8. The

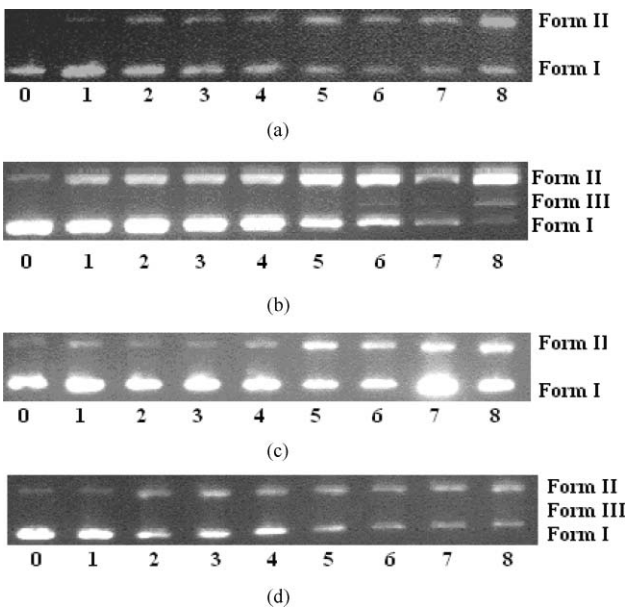

Fig. 7 Agarose gel electrophoresis of pBR322 plasmid DNA treated with complexes at different concentrations. (a) Lane 0: supercoiled DNA (control); lanes 1–8: complex **1** (10, 40, 70, 100, 200, 300, 400, 500 μM). (b) Lane 0: supercoiled DNA (control); lanes 1–8: complex **3** (10, 40, 70, 100, 200, 300, 400, 500 μM). (c) Lane 0: supercoiled DNA (control); lanes 1–8: complex **4** (10, 40, 70, 100, 200, 300, 400, 500 μM). (d) Lane 0: supercoiled DNA (control); lanes 1–8: complex **5** (10, 40, 70, 100, 200, 300, 400, 500 μM).

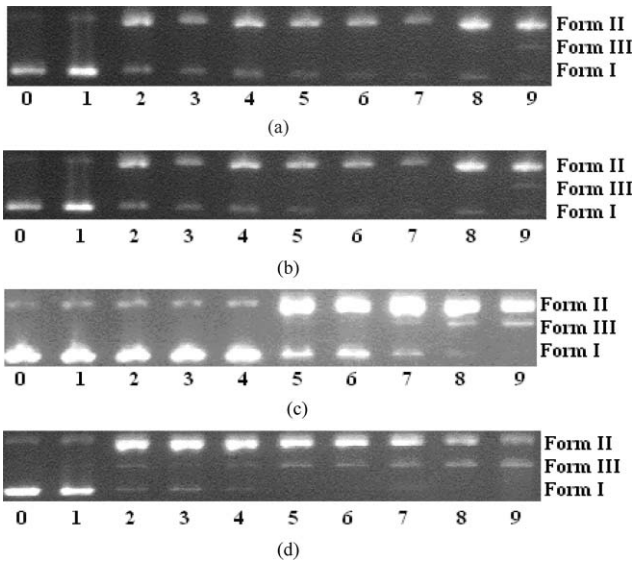

Fig. 8 Agarose gel electrophoresis of pBR322 plasmid DNA treated with complexes with addition of hydrogen peroxide at different concentrations. (a) Lane 0: supercoiled DNA (control); lane 1: H_2O_2 (25 μM); lanes 2–9: H_2O_2 (25 μM) + complex **1** (10, 40, 70, 100, 200, 300, 400, 500 μM). (b) Lane 0: supercoiled DNA (control); lane 1: H_2O_2 (25 μM); lanes 2–9: H_2O_2 (25 μM) + complex **3** (10, 40, 70, 100, 200, 300, 400, 500 μM). (c) Lane 0: supercoiled DNA (control); lane 1: H_2O_2 (25 μM); lanes 2–9: H_2O_2 (25 μM) + complex **4** (10, 40, 70, 100, 200, 300, 400, 500 μM). (d) Lane 0: supercoiled DNA (control); lane 1: H_2O_2 (25 μM); lanes 2–9: H_2O_2 (25 μM) + complex **5** (10, 40, 70, 100, 200, 300, 400, 500 μM).

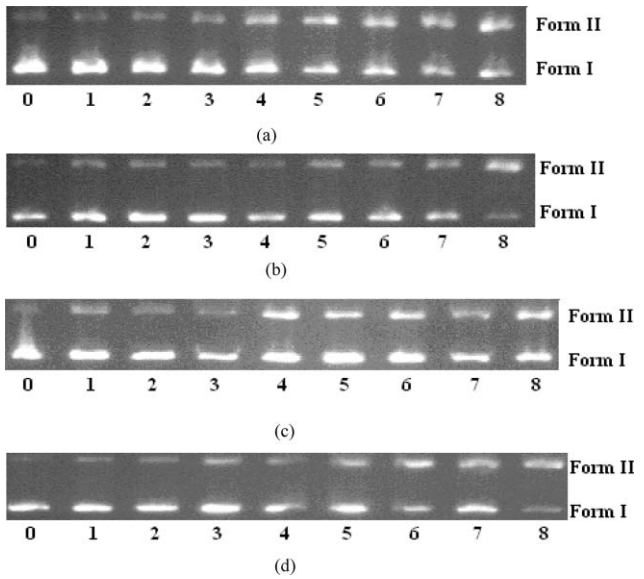

Fig. 9 Agarose gel electrophoresis of pBR322 plasmid DNA treated with 300 μM complexes for different incubation time. (a) Lane 0: supercoiled DNA (control) (10 h); lanes 1–8: complex **1** (0.5, 1, 2, 4, 5, 6, 8, 10 h). (b) Lane 0: supercoiled DNA (control) (10 h); lanes 1–8: complex **3** (0.5, 1, 2, 4, 5, 6, 8, 10 h); (c) Lane 0: supercoiled DNA (control) (10 h); lanes 1–8: complex **4** (0.5, 1, 2, 4, 5, 6, 8, 10 h). (d) Lane 0: supercoiled DNA (control) (10 h); lanes 1–8: complex **5** (0.5, 1, 2, 4, 5, 6, 8, 10 h), respectively.

results indicated that the DNA cleavage activities of the complexes can be promoted in the presence of hydrogen peroxide compared with the case of the absence of hydrogen peroxide under the same experimental conditions (Table S1, ESI†).

A time course of a gel electrophoresis pattern of pBR322 DNA cleavage during a reaction in the presence of 300 μM complex at pH = 7.2 and 37 °C is shown in Fig. 9. With reaction time increase, the amount of Form II increased and Form I gradually disappeared. The results show that all complexes can effectively cleave the pBR322 plasmid DNA without addition of external agents, and cleavages of DNA by the complexes are dependent on the concentrations of complexes and reaction times. From Fig. 10, we can find that all of the processes are typical pseudo-first-order consecutive reactions, which are consistent with the general model for enzyme catalyzed reactions.[32,33] Fitting the experimental data with first-order consecutive kinetic equations, rate constants of 2.11×10^{-5} s^{-1}, 2.34×10^{-5} s^{-1}, 1.48×10^{-5} s^{-1}, 2.27×10^{-5} s^{-1}, for the conversions of supercoiled to nicked DNA are obtained for **1**, **3**, **4** and **5**, respectively. The results indicate that the complex **3** has better nuclease activity than compounds **1**, **4** and **5**.

The DNA cleavage mechanisms by the complexes were investigated in the presence of a hydroxyl radical scavenger (DMSO), a superoxide scavenger (SOD), a singlet oxygen quencher (NaN_3) and a chelating agent (EDTA)[34] under our experimental conditions (Fig. 11, lanes 2–5). The SOD enzyme had no effect on the cleavage reaction (lane 4) suggesting that the superoxide anion is not involved in the cleavage process. Azide (lane 3) inhibits DNA cleavage by the compound indicating that $^1O_2$ is involved in the reaction. The hydroxyl radical scavenger, DMSO (lane 2) diminishes significantly the nuclease activity of the compound which is indicative of the involvement of the hydroxyl radical in the cleavage process. In order to further clarify the cleavage mechanism of pBR322 DNA induced by complexes, it is necessary to perform the cleavage experiment under anaerobic conditions (Fig. S4, lanes 0–2, ESI†), the results show that the complexes hardly cleave pBR322 plasmid DNA under anaerobic conditions. According to the results mentioned above, we propose the hypothesis that the copper(II) complexes examined here may be capable of promoting DNA cleavage through an oxidative DNA damage pathway, in which the active oxygen species involved in the reaction are singlet oxygen, ($^1O_2$) and hydroxyl radical ($^{\bullet}OH$).

Experimental

CAUTION

Perchlorate salts of metal complexes are potentially explosive and therefore should be prepared in small quantities.

Materials and instrumentation

Ligand H_3L (*N*,*N*′-bis(3,5-*tert*-butylsalicylidene-2-hydroxy)-1,3-propanediamine) was synthesized according to a previously reported procedure.[35] Ethidium bromide (EB), calf thymus DNA (CT-DNA) and pBR322 plasmid DNA was from Sigma. Tris-HCl buffer solution was prepared using deionized sonicated triple-distilled water. All other reagents and chemicals were purchased from commercial sources and used as received. Elemental analyses for C, H and N were obtained on a Perkin-Elmer analyzer model 240. Infrared spectroscopy on KBr pellets was performed on a Bruker Vector 22 FT-IR spectrophotometer in the 4000–400 cm^{-1} regions. Electronic spectra were measured on a JASCO V-570 spectrophotometer. Fluorescence spectral data were obtained on

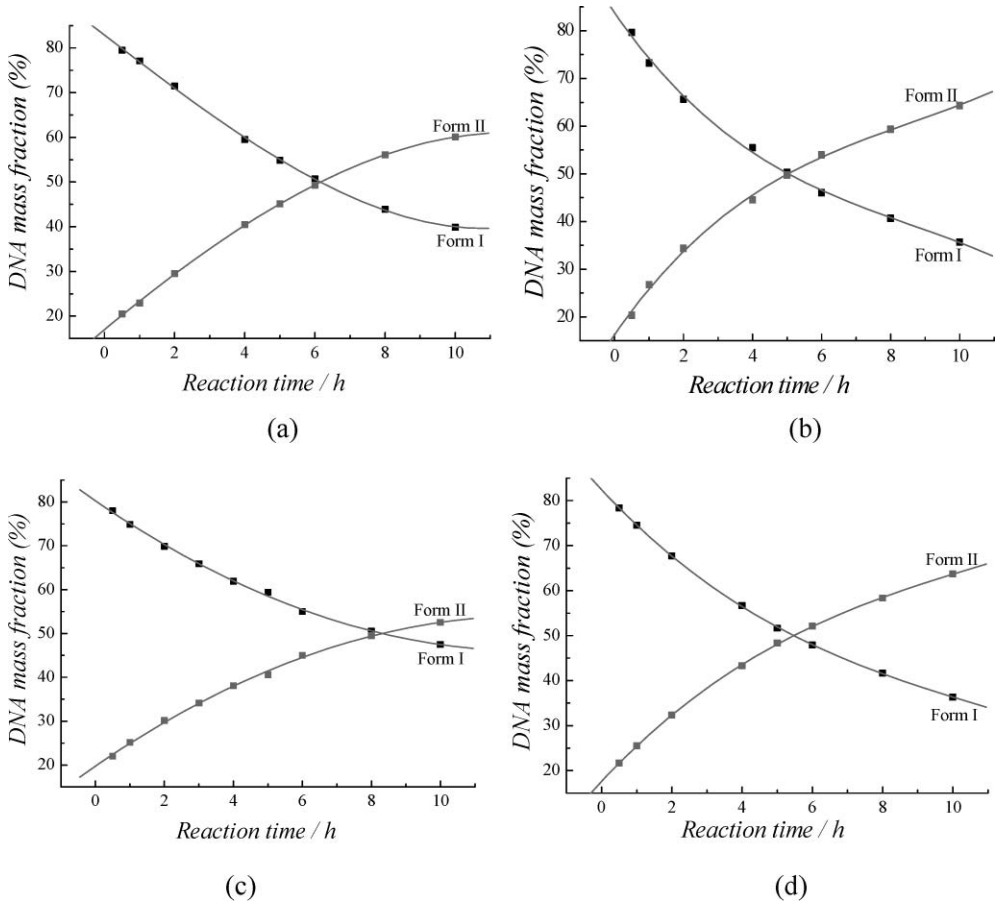

Fig. 10 Agarose gel electrophoresis of pBR322 plasmid DNA treated with 300 μM complexes for different incubation times. Densitometric quantitative results of the gel electrophoresis: (a) complex **1**; (b) complex **3**; (c) complex **4**; (d) complex **5**. Scatter: experimental data, line: fitting curves.

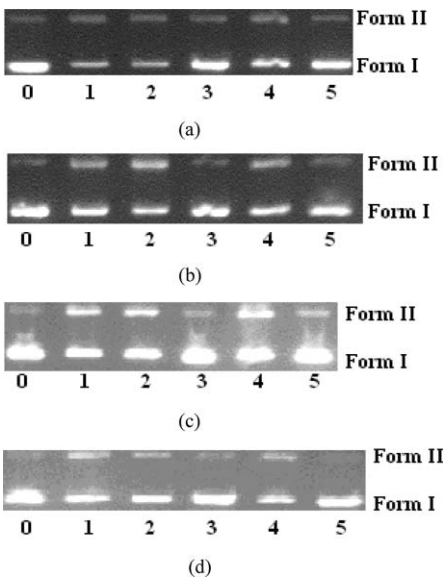

Fig. 11 Agarose gel electrophoresis of pBR322 plasmid DNA treated with 300 μM complex in presence of potential inhibitor agents. Incubation time is 3 h (37 °C): (a) complex **1**; (b) complex **3**; (c) complex **4**; (d) complex **5**. Lane 0: supercoiled DNA (control); lane 1: complex; lane 2: complex + DMSO (1 M), lane 3: complex + NaN_3 (100 mM), lane 4: complex + SOD (15 units); lane 5: complex + EDTA (1 mM).

a MPF-4 fluorescence spectrophotometer at room temperature. Cyclic voltammetry measurements were performed on a BAS Epsilon Electrochemical Workstation. The variable temperature magnetic susceptibility measurements were carried out with microcrystalline samples on a MPMS XL-7 SQUID in the temperature range 2–300 K. Corrections for the diamagnetism were estimated from Pascal's constants. ESR spectra of ground crystals were carried out at X-band with a Bruker ELESYX instrument.

Preparation of complexes

$[Cu_2(L)(OAc)]\cdot 3DMF$ (1). To an acetonitrile solution (10 mL) of $Cu(OAc)_2\cdot H_2O$ (0.4 mmol, 80 mg) was added a 10 mL methanol–DMF (1 : 1) mixture of H_3L (0.2 mmol) and triethylamine (0.6 mmol). The resulting mixture was stirred for 6 h at room temperature. After filtration, green block crystals suitable for X-ray diffraction were obtained by slow evaporation of the filtrate after several days, which were collected by filtration, washed with diethyl ether and dried in air (yield: 32 mg, 40%). Elemental analysis (%): calc. for $C_{44}H_{73}Cu_2N_5O_8$: C, 57.00; H, 7.94; N, 7.55. Found: C, 57.02; H, 8.01; N, 7.50.

$[Cu_2(L)(OAc)]_2\cdot 3DMF$ (2). To an acetonitrile solution (10 mL) of $Cu(OAc)_2\cdot H_2O$ (0.4 mmol, 80 mg) was added 5 mL DMF of H_3L (0.2 mmol) and triethylamine (0.6 mmol). The resulting mixture was stirred for 4 h at room temperature. After filtration,

green block crystals suitable for X-ray diffraction were obtained by slow evaporation of the filtrate after several months, which were collected by filtration, washed with diethyl ether and dried in air (yield: 24 mg, 30%). Elemental analysis (%): calc. for $C_{79}H_{121}Cu_4N_7O_{13}$: C, 58.18; H, 7.48; N, 6.01. Found: C, 58.20; H, 7.44; N, 6.03.

[Cu_2(L)(BNPP)]·3CH_3CN (3). To an acetonitrile solution (5 mL) of $Cu(ClO_4)_2·6H_2O$ (0.4 mmol, 144.8 mg) was added 10 mL CH_3CN–DMF (1 : 1) of H_3L (0.2 mmol) and triethylamine (0.6 mmol). Then 0.2 mmol BNPP and 0.2 mmol NEt_3 dissolved in 3 mL CH_3CN was added to the above mixture after stirring for 1 h at room temperature. The green solution was stirred for another 3 h. After filtration, green block crystals suitable for X-ray diffraction were obtained by slow evaporation of the filtrate after several months, which were collected by filtration, washed with diethyl ether and dried in air (yield: 65.2 mg, 45%). Elemental analysis (%): calc. for $C_{51}H_{64}Cu_2N_7O_{11}P$: C, 55.23; H, 5.82; N, 8.84. Found: C, 55.20; H, 5.86; N, 8.81.

[Cu_2(L)(Fa)]·2DMF (4). Complex **4** was prepared similarly to **3**, but adding 0.2 mmol 2-tetrahydrofuroic acid instead of BNPP to the reaction mixture. After filtration, green block crystals suitable for X-ray diffraction were obtained by slow evaporation of the filtrate after several months, which were collected by filtration, washed with diethyl ether and dried in air (yield: 72.4 mg, 50%). Elemental analysis (%): calc. for $C_{44}H_{68}Cu_2N_4O_8$: C, 58.19; H, 7.55; N, 6.17. Found: C, 58.22; H, 7.53; N, 6.19.

[Cu_2(L)(Pa)]·DMF (5). Complex **5** was prepared similarly to **3**, but adding 0.2 mmol PhCOONa instead of BNPP and NEt_3 to the reaction mixture. After filtration, green block crystals suitable for X-ray diffraction were obtained by slow evaporation of the filtrate after several days, which were collected by filtration, washed with diethyl ether and dried in air (yield: 60.8 mg, 42%). Elemental analysis (%): calc. for $C_{43}H_{58.50}Cu_2N_3O_6$: C, 61.44; H, 7.02; N, 5.00. Found: C, 61.50; H, 6.99; N, 4.98.

X-Ray crystallography

Diffraction data for **1**, **2**, **4** and **5** were collected at 113 (2) K and **3** at 293 (2) K, with a Rigaku Saturn CCD diffractometer using Mo-Kα radiation (λ = 0.71073 Å) with the ω–2θ scan technique. An empirical absorption correction was applied to the raw intensities.[36] The structures were solved by direct methods (SHELX-97) and refined with full-matrix least-squares technique on F^2 using SHELX-97.[37,38] The hydrogen atoms were added theoretically, and riding on the concerned atoms and refined with fixed thermal factors. The details of crystallographic data and structure refinement parameters are summarized in Table 1.

DNA-binding and cleavage experiments

The UV absorbance at 260 and 280 nm of the CT-DNA solution in 18 mM NaCl–50 mM Tris–HCl buffer (pH = 7.2) give a ratio of 1.8–1.9, indicating that the DNA was sufficiently free of protein.[33] The concentration of CT-DNA was determined from its absorption intensity at 260 nm with a molar extinction coefficient of 6600 M^{-1} cm^{-1}.[39] The absorption spectra of **1**, **3**, **4** and **5** binding to DNA were performed by increasing amount of CT-DNA to the complexes in Tris-HCl buffer (pH = 7.2).

The relative bindings of **1**, **3**, **4** and **5** to CT-DNA were studied with an EB–DNA solution in Tris-HCl/NaCl buffer (pH = 7.2). The fluorescence spectra were recorded at room temperature with excitation at 510 nm and emission at 602 nm. Such experiments were carried out by titrating complexes into EB–DNA solution containing 4.0×10^{-6} M EB and 80×10^{-6} M of DNA.

The DNA cleavage experiments were done by agarose gel electrophoresis, which was performed by incubation at 37 °C for 3 h as follows: pBR322DNA (0.1 μg μL^{-1}) in 50 mM Tris–HCl/18 mM NaCl buffer (pH = 7.2) was treated with complex in the absence of additives. The samples were incubated for 3 h, and then loading buffer was added. Then the samples were electrophoresed for 4 h at 80 V on 0.8% agarose gel using Tris–boric acid–EDTA buffer. After electrophoresis, bands were visualized by UV light and photographed. Quantification of cleavage products was performed by UVIpro software, Version 10.03.[40] Supercoiled plasmid DNA values were corrected by a factor of 1.3, based on average literature estimate of lowered binding of ethidium.[41]

Cleavage mechanistic investigations of pBR322 DNA were done using different reagents such as DMSO, NaN_3, SOD and EDTA added to pBR322 DNA prior to the addition of complex. The anaerobic conditions were achieved using an MBRAUN LAB-Star glove box. Deoxygenated solutions were prepared by four freeze–pump–thaw cycles. Before each cycle the solutions were equilibrated with nitrogen to aid the deoxygenation process. The deoxygenated solutions were stored under a nitrogen atmosphere prior to use. Reaction mixtures were prepared in a glove box by addition of the appropriate volumes of stock solutions to the reaction tubes.

Conclusions

In summary, we have synthesized and characterized five binuclear copper(II) complexes with Schiff base ligand H_3L. Variable-temperature magnetic susceptibility studies (2–300 K) indicate the existence of ferromagnetic coupling between the copper(II) ions in complexes **1** and **4**, and antiferromagnetic coupling in complexes **3** and **5**, and have a clear dependence on Cu–O(μ-alkoxo)–Cu angles. The complexes can all effectively promote cleavage of plasmid DNA without addition of external agents and in the presence of hydrogen peroxide at pH = 7.2 and 37 °C. DNA cleavage mechanism studies show that complexes examined here may be capable of promoting DNA cleavage through an oxidative DNA damage pathway.

Abbreviations

EB	ethidium bromide
Tris	tris(hydroxymethyl)aminomethane
EDTA	ethylenediaminetetraacetic acid
DMSO	dimethyl sulfoxide
CT-DNA	calf thymus DNA
TBE	Tris-boracic-EDTA

Acknowledgements

This work was supported by the National Natural Science Foundation of China (No. 20771063).

References

1 S. Ferrer, R. Ballesteros, A. Sambartolome, M. Gonzalez, G. Alzuet, J. Borras and M. Liu, *J. Inorg. Biochem.*, 2004, **98**, 1436.
2 D. S. Sigman and C. H. B. Chen, in *Metal–DNA Chemistry*, ed. T. D. Tulius, ACS Symposium Series 402, American Chemical Society, Washington, DC, 1989.
3 E. L. Hegg and J. N. Burstyn, *Inorg. Chem.*, 1996, **35**, 7474.
4 K. Dhara, P. Roy, J. Ratha, M. Manassero and P. Banerjee, *Polyhedron*, 2007, **26**, 4509.
5 F. Mancin, P. Scrimin, P. Tecilla and U. Tonellato, *Chem. Commun.*, 2005, 2540.
6 K. E. Erkkila, D. T. Odom and J. K. Barton, *Chem. Rev.*, 1999, **99**, 2777.
7 G. Pratviel, J. Bernadou and B. Meunier, *Adv. Inorg. Chem.*, 1998, **45**, 251.
8 M. M. Meijler, O. Zelenko and D. S. Sigman, *J. Am. Chem. Soc.*, 1997, **119**, 1135.
9 M. G. Álvarez, G. Alzuet, J. Borrás, B. Macías and A. Castiñeiras, *Inorg. Chem.*, 2003, **42**, 2992.
10 Q. Jiang, N. Xiao, P. F. Shi, Y. G. Zhu and Z. J. Gou, *Coord. Chem. Rev.*, 2007, **251**, 1951.
11 Q. Zhu, Y. X. Lian, S. Thyagarajan, S. E. Rokita, K. D. Karlin and N. V. Blough, *J. Am. Chem. Soc.*, 2008, **130**, 6304, and references therein.
12 C. H. Kao, H. H. Wei, Y. H. Liu, G. H. Lee, Y. Wang and C. J. Lee, *J. Inorg. Biochem.*, 2001, **84**, 171.
13 S. C. Cheng and H. H. Wei, *Inorg. Chim. Acta.*, 2002, **340**, 105.
14 C. H. Weng, S. C. Cheng, H. M. Wei, H. H. Wei and C. J. Lee, *Inorg. Chim. Acta*, 2006, **359**, 2029.
15 W. Mazurek, B. J. Kennedy, K. S. Murray, M. J. O'Connor, J. R. Rodgers, M. R. Snow, A. G. Wedd and P. R. Zwack, *Inorg. Chem.*, 1985, **24**, 3258.
16 J. Reim and B. Krebs, *J. Chem. Soc., Dalton Trans.*, 1997, 379.
17 J. Qian, W. Gu, H. Liu, F. X. Gao, L. Feng, S. P. Yan, D. Z. Liao and P. Cheng, *Dalton Trans.*, 2007, 1060.
18 H. D. Bian, W. Gu, J. Y. Xu, F. Bian, S. P. Yan, D. Z. Liao, Z. H. Jiang and P. Cheng, *Inorg. Chem.*, 2003, **42**, 4265.
19 Y. C. Chu, S. F. Huang, R. Koner, G. H. Lee, Y. Wang, S. Mohanta and H. H. Wei, *Inorg. Chem.*, 2004, **43**, 2759.
20 P. E. Kruger, B. Moubaraki, G. D. Fallon and K. S. Murray, *J. Chem. Soc., Dalton Trans.*, 2000, 713.
21 R. Fortea, P. Alemany, S. Alvarez and E. Ruiz, *Inorg. Chem.*, 2002, **41**, 3769.
22 G. Speie, J. Csihony, A. M. Whalen and C. G. Pierpont, *Inorg. Chem.*, 1996, **35**, 3519.
23 J. L. Mesa, J. L. Pizarro and M. I. Arriortua, *Cryst. Res. Technol.*, 1998, **33**, 489.
24 A. A. El-Asmy and G. A. A. Al-Hazmi, *Spectrochim. Acta, Part A*, 2009, **71**, 1885.
25 D. Kivelson and R. Neiman, *J. Chem. Phys.*, 1961, **35**, 149.
26 M. Gaber, K. Y. El-Baradie and Y. S. Y. El-Sayed, *Spectrochim. Acta, Part A*, 2008, **69**, 534.
27 V. T. Kasumo, *Spectrochim. Acta, Part A*, 2001, **57**, 1649.
28 V. A. Bloomfield, D. M. Crothers and I. Tinocco Jr, *Physical Chemistry of Nucleic Acids*, Harper & Row, New York, 1974, p. 432.
29 J. R. Lakowicz and G. Webber, *Biochemistry*, 1973, **12**, 4161.
30 T. F. Miao, L. Qian, S. Y. Liao, H. L. Lu, K. C. Zheng and L. N. Ji, *J. Inorg. Biochem.*, 2008, **870**, 94.
31 X. L. Wang, H. Chao, H. Li, X. L. Hong, L. N. Ji and X. Y. Li, *J. Inorg. Biochem.*, 2004, **98**, 423.
32 D. M. Kong, J. Wang, L. N. Zhu, Y. W. Jin, X. Z. Li, H. X. Shen and H. F. Mi, *J. Inorg. Biochem.*, 2008, **102**, 824.
33 J. J. Li, R. Geyer and W. Tan, *Nucleic Acid Res.*, 2000, **28**, e52.
34 M. E. Reichmann, S. A. Rice, C. A. Thomas and P. Doty, *J. Am. Chem. Soc.*, 1954, **76**, 3047.
35 M. Tsuchimoto, T. Ishii, T. Imaoka and K. Yamamoto, *Bull. Chem. Soc. Jpn.*, 2004, **77**, 1849.
36 G. M. Sheldrick, *Correction Software*, University of Göttingen, Germany, 1996.
37 G. M. Sheldrick, *SHELXS 97, Program for the Solution of Crystal Structures*, University of Göttingen, Germany,1997.
38 G. M. Sheldrick, *SHELXL 97, Program for the Refinement of Crystal Structures*, University of Göttingen, Germany, 1997.
39 J. Marmur, *J. Mol. Biol.*, 1961, **3**, 585.
40 (*a*) R. P. Herzberg and P. P. Derwan, *J. Am. Chem. Soc.*, 1982, **104**, 313; (*b*) C. K. Mirabelli, C. H. Huang and S. T. Crooke, *Cancer Res.*, 1980, **40**, 4173; (*c*) C. A. Detmer, F. V. Pamatong and J. R. Borcarsly, *Inorg. Chem.*, 1996, **35**, 6292.
41 F. V. Pamatong, C. A. Detmer and J. R. Bocarsly, *J. Am. Chem. Soc.*, 1996, **118**, 5339.

